Journal of Molecular Liquids 304 (2020) 112778

Contents lists available at ScienceDirect

Journal of Molecular Liquids

journal homepage: www.elsevier.com/locate/molliq

Thermophysical study of the binary mixtures of triethyl phosphate with *N*-methylformamide, *N*,*N*-dimethylformamide and *N*,*N*-dimethylacetamide – Experimental and theoretical approach

Dorota Warmińska *, Maciej Śmiechowski

Department of Physical Chemistry, Chemical Faculty, Gdańsk University of Technology, 80-233 Gdańsk, Poland

ARTICLE INFO

Article history:
Received 16 September 2019
Received in revised form 17 January 2020
Accepted 24 February 2020
Available online 25 February 2020

Keywords:
Excess properties
Triethyl phosphate
N-methylformamide
N,*N*-dimethylformamide
N,*N*-dimethylacetamide
Molecular dynamics simulations

ABSTRACT

Densities at (293.15, 298.15, 303.15 and 308.15) K, and viscosities and ultrasonic velocities at 298.15 K of binary liquid mixtures of triethyl phosphate with *N*-methylformamide, *N*,*N*-dimethylformamide and *N*,*N*-dimethylacetamide have been measured over the entire range of composition at $p = 0.1$ MPa. From the experimental data, values of excess molar volume, excess isentropic compressibility, viscosity deviation and excess Gibbs energy of activation for viscous flow have been calculated. These results were fitted to the Redlich-Kister-type polynomial equation. The viscosity deviations and the excess Gibbs energy were found to be positive for the all systems investigated, while the excess volumes and the excess isentropic compressibilities were negative for TEP + DMA and for TEP + DMF systems, and positive for mixtures TEP + NMF. These results were interpreted based on the strength of the specific interaction, size and shape of molecules. Molecular dynamics simulations were used to provide a detailed explanation of the differences between the TEP + NMF and other systems, which were ultimately traced to strong hydrogen bonding between NMF and TEP.

1. Introduction

Since mixed solvents offer a wide range of desired properties, they are frequently used as reaction media for many chemical, industrial and biological processes. Thus, the knowledge of the thermodynamic properties of binary and ternary systems involving organic solvents is essential not only from theoretical point of view, but also for proper design of industrial processes. The derived deviations or excess properties obtained from the experimental data on density, viscosity and ultrasonic velocity provide valuable information about the structure of liquids and intermolecular interactions in liquid mixtures. Moreover, the knowledge of the experimental data on these physicochemical properties themselves allows to modify and obtain the desired properties of solvent mixtures for specific application. Simultaneously, molecular simulations offer a possibility to explain the experimentally measured properties on the basis of the intermolecular interactions in the system studied on a microscopic scale.

In this study triethyl phosphate (TEP) is chosen as a solvent due to the recent interest in its application as a non-flammable electrolyte in lithium-ion batteries and due to the use of TEP as an industrial reagent for the production of polyvinylidene fluoride (PVDF) microporous membranes [1,2]. In both applications, the mixtures of triethyl phosphate with organic solvents have been experimented with. In PVDF microporous membranes production, the use of triethyl phosphate and *N*,*N*-dimethylacetamide (DMA) mixtures has allowed to control the membrane morphology [3]. In lithium-ion batteries, by the addition of the second solvent the decomposition of triethyl phosphate, which disturbed the reaction between lithium ions and the anode, was avoided [4,5]. Taking these effects into account, we decided to investigate the thermodynamical behavior and microstructure of binary mixtures of triethyl phosphate with *N*-methylformamide (NMF), *N*,*N*-dimethylformamide (DMF) and *N*,*N*-dimethylacetamide, which had not been studied before. To the best of our knowledge only the densities of triethyl phosphate with water and hexamethylphosphoric triamide have been measured so far [6,7].

In the present study, we have measured the densities at (293.15, 298.15, 303.15 and 308.15) K, as well as viscosities and ultrasonic velocities at 298.15 K for the liquid mixtures of TEP and amides over the entire range of their compositions. From the experimental data, values of excess molar volume, excess isentropic compressibility, viscosity deviation and excess Gibbs energy of activation for viscous flow for these systems have been calculated. The significance of the obtained parameters has been emphasized for the understanding of the intermolecular interactions between triethyl phosphate and amides molecules. Moreover, molecular dynamics (MD) simulations of the studied systems at 298.15 K over the entire composition range

* Corresponding author.
E-mail address: dorwarmi@pg.edu.pl (D. Warmińska).

https://doi.org/10.1016/j.molliq.2020.112778

allowed us to highlight the crucial differences between the TEP + NMF system and other amides and pinpoint their origin at the strong hydrogen bonding (H-bonding) in the case of NMF.

2. Experimental and computational details

2.1. Materials

The chemicals in this study, triethyl phosphate, *N*-methylformamide, *N*,*N*-dimethylformamide and *N*,*N*-dimethylacetamide were purchased from Sigma-Aldrich and they were used as received from the supplier. Table 1 presents the corresponding information. The average water content in the reagents was measured by the Karl Fischer titration method (831 KF coulometer apparatus from Metrohm).

Table 2 shows the thermophysical properties of the used materials at work temperatures and at atmospheric pressure ($p = 0.1$ MPa) together with the comparison with literature data at 298.15 K. As seen, the experimental values of density, sound velocity and viscosity obtained for pure solvents were in good agreement with the values found in the literature.

The mixtures for measurements were prepared by mass and were kept in special airtight stopper glass bottles to avoid evaporation. The weighing was done by using an analytical balance (Mettler Toledo) with the precision of 0.1 mg. The uncertainty in the mole fraction was estimated to be less than $\pm 1 \cdot 10^{-4}$.

2.2. Measurements

The densities of the binary mixtures were measured at different temperatures with a digital vibration-tube analyzer (Anton Paar DMA 5000, Austria) with proportional temperature control that kept the samples at working temperature with an accuracy of 0.01 K. Prior to each series of measurements, the apparatus was calibrated using double distilled and degassed water, and with dry air at atmospheric pressure (0.1 MPa). The experimental uncertainty of the density measurement was better than 0.035 $kg \cdot m^{-3}$.

The sound velocity was determined using the sound analyzer OPTIME 1.0 from OPTEL (Poland) with an uncertainty of 0.15 $m \cdot s^{-1}$ by measuring the time it takes for a pulse of ultrasound to travel from one transducer to another (*pitch-catch*) or to return to the same transducer (*pulse-echo*). The cell was thermostated at 298.15 ± 0.01 K and calibrated with double distilled water, with the value 1496.69 $m \cdot s^{-1}$ used as the sound velocity in pure water at 298.15 K.

The viscosity measurements were carried out using an Ubbelohde type suspended level capillary viscometer, which was calibrated with doubly distilled deionized water at 298.15 K. A thoroughly cleaned and perfectly dried viscometer filled with experimental liquid was placed vertically in a glass sided water thermostat with precision ± 0.05 K. After attaining thermal equilibrium the efflux time was measured with a digital stopwatch with the resolution of 0.01 s. An average of three or four readings reproducible within 0.1 s was used as the final efflux time. The estimated uncertainty for the viscosity was ± 0.01 mPa·s.

2.3. Computational details

Molecular dynamics (MD) simulations were performed using the GROMACS 5.1.2 software package [23]. The simulated systems were composed of 1000 solvent molecules (TEP (1) + DMA, DMF, or NMF (2)) and the compositions studied were $x_1 = 0.0$, 0.1, 0.2, 0.3, 0.4, 0.5, 0.6, 0.7, 0.8, 0.9, and 1.0. The initial cubic box length varied from ~5.0 to ~6.5 nm, depending on the TEP content, and periodic boundary conditions were imposed. The starting system configurations were prepared using GROMACS solvation tools (i.e., gmx insert-molecules and gmx solvate). The NMF molecules were introduced in the *trans* peptide bond configuration and remained in this configuration throughout the entire simulations. The force field parameters for all solvents were taken from the flexible, all-atom OPLS-AA force field [24,25] and parameter files and initial equilibrated configurations of pure solvent boxes were obtained from the GROMACS solvents database [10,26]. Electrostatic interactions were evaluated using the smooth particle-mesh Ewald method [27] with a real-space cut off set to 1.2 nm and a grid spacing of ~0.1 nm. The van der Waals interactions were smoothly switched off starting at 1.0 nm to the final cut off of 1.2 nm. The computational efficiency for the short-ranged non-bonded interactions was enhanced by using Verlet neighbor lists with automatic buffering [28].

Following initial energy minimalization using the steepest descent algorithm with the 10 $kJ\ mol^{-1}\ nm^{-1}$ convergence criterion for maximum force, further MD simulations were performed using the velocity Verlet algorithm for the integration of the equations of motion [29] with the time step of 0.5 fs. The isothermal–isobaric (NPT) ensemble was sampled by keeping the temperature at 298.15 K with the aid of the Nosé–Hoover extended ensemble method [30,31] and the pressure at 1 bar using the Martyna–Tuckerman–Tobias–Klein barostat [32,33]. The coupling constants were set to 0.5 ps and 3 ps for the thermostat and barostat, respectively. The isothermal compressibility for the barostat was set to $5.8 \cdot 10^{-10}\ Pa^{-1}$ (the liquid TEP compressibility from MD simulations [10]). The 10 ns ($20 \cdot 10^6$ steps) equilibration run was followed by the 30 ns ($60 \cdot 10^6$ steps) production run used to obtain ensemble averages of the studied properties, with data acquisition every 1 ps (every 2000 steps) for atomic coordinates and velocities and every 0.1 ps (every 200 steps) for energy and related properties.

For hydrogen bonding and vibrational density of states (VDOS) analyses that require frequent sampling, we additionally used a further canonical (NVT) ensemble run of 1 ns ($2 \cdot 10^6$ steps) length and at the cell volume equal to the average from the NPT production run, followed by a microcanonical (NVE) ensemble run of 0.1 ns ($2 \cdot 10^5$ steps) length during which data were sampled every 8 steps (i.e., every 4 fs). The NVT ensemble was introduced by removing the coupling to the barostat, whereas in the NVE ensemble also the coupling to the thermostat was removed. We used standard GROMACS tools for analysing the trajectories, i.e., gmx rdf for radial distribution functions, gmx dos for VDOS and gmx hbond for hydrogen bonding-related properties.

3. Results and discussion

3.1. Excess molar volume

Experimental values of density and calculated values of excess molar volume for the binary systems of triethyl phosphate with *N*-

Table 1
Provenance and mass fraction purity of the compounds studied.

Chemical name	Source	CAS number	Purity/mass fraction[a]	Water content/10^6 $w(H_2O)$[b]
Triethyl phosphate	Sigma Aldrich	78-40-0	≥0.998	355
N,*N*-dimethylacetamide	Sigma Aldrich	127-19-5	≥0.995	322
N,*N*-dimethylformamide	Sigma Aldrich	68-12-2	≥0.998	172
N-methylformamide	Sigma Aldrich	123-39-7	0.99	223

[a] As stated by the supplier.
[b] Karl Fisher titration.

Table 2
Thermophysical properties of the pure compounds at $p = 0.1$ MPa and at work temperatures and comparison of densities, sound velocities and dynamic viscosities with literature data at $T = 298.15$ K.[a]

T/K	d/(kg·m^{-3})		u/(m·s^{-1})		η/(mPa·s)		$10^3\alpha$/(K^{-1})	C_p/(J·K^{-1}·mol^{-1})
	Exptl.	Lit.	Exptl.	Lit.	Exptl.	Lit.		
Triethyl phosphate								
	1069.002							
293.15								
	1064.005	1064[b], 1064.189[c]	1236.47	1236.46[c]	1.503	1.548[b], 1.700[d]	0.937	333.3[e]
298.15								
	1059.003							
303.15								
	1053.995							
308.15								
N,*N*-dimethylacetamide								
	940.906							
293.15								
	936.284	936.29[f], 936.281[g]	1455.67	1455.82[g], 1455.37[c]	0.917	0.920[h], 0.923[i]	0.985	176.0[j]
298.15								
	931.666							
303.15								
	927.047							
308.15								
N,*N*-dimethylformamide								
	948.613							
293.15								
	943.845	943.85[k], 943.913[g]	1456.93	1457.17[g], 1457.13[l]	0.792	0.791[m], 0.796[h]	1.010	148.3[j]
298.15								
	939.069							
303.15								
	934.284							
308.15								
N-methylformamide								
	1003.251							
293.15								
	998.894	999.2[n], 998.8[o]	1431.51	1430.7[n], 1431.2[p]	1.695	1.681[o], 1.653[r]	0.870	123.8[j]
298.15								
	994.540							
303.15								
	990.185							
308.15								

[a] Standard uncertainties u are u(T)=0.01 K for densities and sound velocities and u(T) = 0.05 K for viscosities, u(p) = 0.01 MPa, u(d) = 0.035 kg·m^{-3}, u(u) =0.15 m·s^{-1} and u(η) =0.01 mPa·s.
[b] Ref. [7].
[c] Ref. [8].
[d] Ref. [9].
[e] Ref. [10].
[f] Ref. [11].
[g] Ref. [12].
[h] Ref. [13].
[i] Ref. [14].
[j] Ref. [15].
[k] Ref. [16].
[l] Ref. [17].
[m] Ref. [18].
[n] Ref. [19].
[o] Ref. [20].
[p] Ref. [21].
[r] Ref. [22].

methylformamide, *N*,*N*-dimethylformamide and *N*,*N*-dimethylacetamide are collected in Table S1 in Supplementary material. The values of excess molar volumes were calculated using the following equation:

$$V^E = \sum_i x_i M_i \left(\frac{1}{d} - \frac{1}{d_i}\right) \quad (1)$$

where d is the density of the mixture and x_i, M_i, and d_i are, the mole fraction, the molar mass and density of component i, respectively.

The plots of V^E against mole fraction of triethyl phosphate, x_1, for the binary mixtures at 298.15 K are presented in Fig. 1. As it can be observed, over the whole composition range studied the excess molar volume is found to be negative for the binary mixtures containing triethyl phosphate and *N*,*N*-dimethylformamide or *N*,*N*-dimethylacetamide and positive for the mixture of triethyl phosphate with *N*-methylformamide. Moreover, the magnitude of the values of V^E obtained for the TEP + NMF system is significantly bigger than for TEP + DMA/DMF systems. This result can be interpreted based on the strength of the specific interaction, size and shape of molecules. It is well known, that the sign and magnitude of the value of the excess molar volume of a system are the result of two competing factors: expansion and contraction occurring in the mixing process. If strong interactions, such as heteromolecular association through the formation of hydrogen bond, dipole-dipole interactions, and also steric effects allowing accommodation of one component molecules into the other's

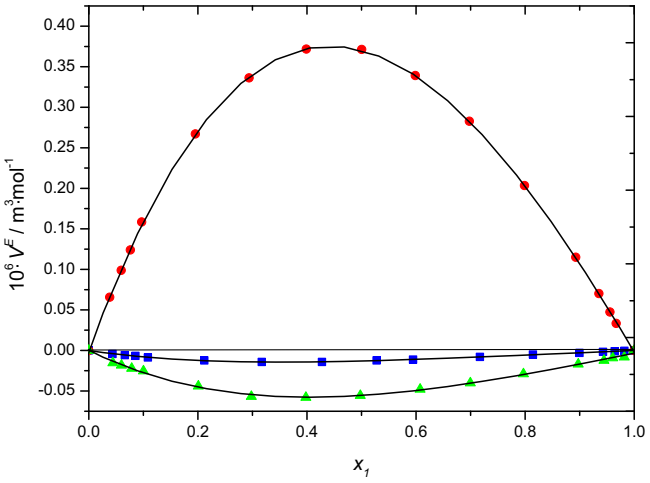

Fig. 1. Excess molar volumes, V^E, for triethyl phosphate (1) + amide (2) at $p = 0.1$ MPa as a function of mole fraction, x_1, at $T = 298.15$ K: ● (red), *N*-methylformamide; ■ (blue), *N*,*N*-dimethylacetamide; ▲ (green), *N*,*N*-dimethylformamide; —, Eq. (6).

structure dominate, then V^E values become negative. If the dispersion forces, dissociation of a component which is associated in pure state, and the unfavorable packing of the unlike molecules are main effects, then excess molar volume values become positive [34].

Among the solvents studied only *N*-methylformamide is strongly self-associated through hydrogen bonding and dipole–dipole interactions (μ = 3.86 D) [35]. Triethyl phosphate and *N*,*N*-dimethylformamide or *N*,*N*-dimethylacetamide lack any significant liquid structural effects due to the absence of hydrogen bonds, although evidence for dipole–dipole self-association in pure DMF, DMA and TEP has been reported [36–38].

Furthermore, it is has been established that triethyl phosphate has strong hydrogen bond acceptor capability and it is able to form hydrogen bonds with strong H-bond donors like water and methanol [27,39,40]. Thus, one can suspect that, apart from dipole–dipole interactions, also H-bonds of the N–H···O=P type are possible between TEP and NMF molecules.

In contrast, for the systems TEP + DMF and TEP + DMA very small negative deviations from ideal behavior are observed, probably because the molecular structures and characteristics of the two components are similar. The less negative excess molar volumes observed for mixtures of triethyl phosphate with *N*,*N*-dimethylacetamide than those for *N*,*N*-dimethylformamide can be the result of better geometrical fitting and smaller difference of the dipole moments of TEP and DMA molecules.

Fig. 2 shows the excess molar volumes for triethyl phosphate and *N*,*N*-dimethylacetamide system at all temperature studied. As is seen, an increase in temperature (293.15 to 308.15) K, results in a decrease of the excess molar volumes over the entire range of concentration of triethyl phosphate. Moreover, the same result was observed for TEP + NMF and TEP + DMF mixtures (Table S1). The contraction in V^E values with temperature increase seems to suggest that the increasing temperature causes a greater dissociation effect on the amide–amide or TEP–TEP self-associates than on the dissociation of the TEP–amide complexes.

3.2. Excess isentropic compressibility

The isentropic compressibilities of mixtures of solvents were estimated using experimental values of densities and sound velocities by the Laplace equation, providing the link between thermodynamics and acoustics.

$$\kappa_S = 1/(u^2 d), \tag{2}$$

Then, according the approach developed by Benson et al., the excess isentropic compressibility was calculated as,

$$\kappa_S^E = \kappa_S - \sum_i \phi_i \kappa_{S,i} - T\sum_i \phi_i V_i \alpha_i^2 / C_{p,i} + T\sum_i x_i V_i, \tag{3}$$

where Φ_i, V_i, α_i, $C_{p,i}$ and $\kappa_{S,i}$ are the volume fraction, defined as $\phi_i = x_i V_i / \sum_i x_i V_i$, the molar volume, isobaric thermal expansibility, the molar heat capacity at constant pressure and the isentropic compressibility of pure component *i*, respectively [41]. The values of molar heat capacities at constant pressure for the investigated liquids were taken from the literature [10,15] The isobaric thermal expansibility values were predicted

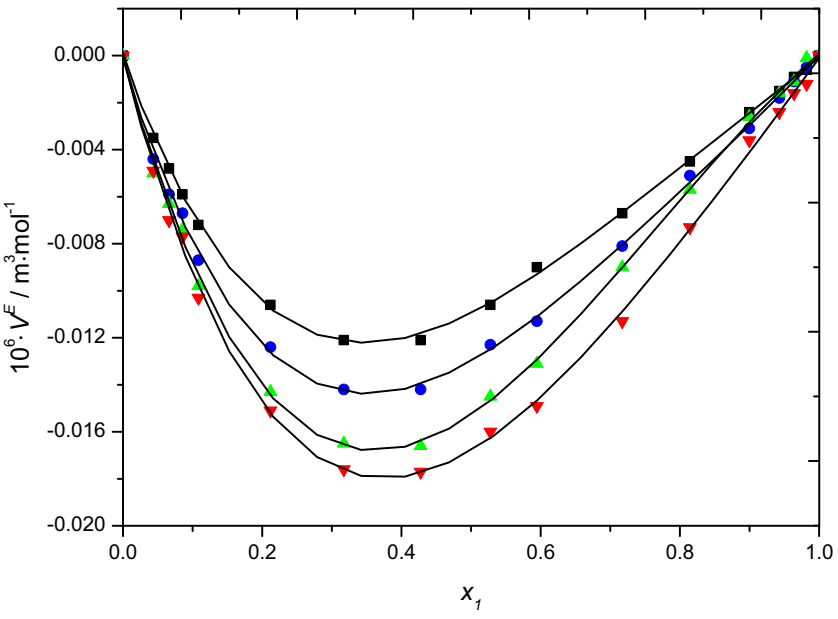

Fig. 2. Excess molar volumes, V^E, for triethyl phosphate (1) + *N*,*N*-dimethylacetamide (2) at $p = 0.1$ MPa as a function of mole fraction, x_1 at: ■ (black), $T = 293.15$ K; ● (blue), $T = 298.15$ K; ▲ (green), $T = 303.15$ K; ▼ (red), $T = 308.15$ K; —, Eq. (6).

by using experimental density data, and together with the C_p values are recorded in Table 2.

Table S2 in Supplementary material presents experimental values of sound velocity and calculated values of excess isentropic compressibility for the binary systems of triethyl phosphate with *N*-methylformamide, *N*,*N*-dimethylformamide and *N*,*N*-dimethylacetamide at 298.15 K.

Fig. 3 shows the excess isentropic compressibility as a function of the molar fraction for all systems studied. As is seen, for the mixtures containing *N*,*N*-dimethylformamide or *N*,*N*-dimethylacetamide the values of $\kappa_S^E$are negative over the entire composition range and they are more negative for the TEP + DMF system. For mixtures containing NMF positive excess isentropic compressibility values are observed.

Thus, the behavior of the excess isentropic compressibility seems to be consistent with the obtained values of excess molar volume. The positive values of κ_S^E obtained for the TEP + NMF system indicate that the mixture is more compressible than the corresponding ideal mixture. As discussed above, when TEP is added to NMF the hydrogen bonds in the latter are disturbed, and dipole–dipole interactions and hydrogen bonds between unlike molecules are formed.

The negative values of κ_S^E obtained for the systems TEP + DMA/DMF suggest that the contribution of dipole–dipole interactions and molecular packing is more than that of the rupture of associated entities. Thus, the mixtures contain relatively less compressible structure as compared to that in the pure solvents.

Moreover, more negative values of the excess isentropic compressibilities observed for TEP + DMF system in comparison to those for TEP + DMA mixtures may be due to the stronger interactions between triethyl phosphate and *N*,*N*-dimethylformamide than those between triethyl phosphate and *N*,*N*-dimethylacetamide molecules. It seems to be the result of the presence of methyl group at carbonyl carbon in DMA, which causes greater electron density at carbonyl oxygen atom in DMA than that in DMF and makes *N*,*N*-dimethylacetamide interact weaker with TEP. Another reason for smaller deviations from the ideal mixture observed for TEP + DMA system can be smaller difference in the free volumes of pure species (85.08 Å^3) compared to that in TEP + DMF mixture (121.56 Å^3) [42]. It has been established that as the difference of the free volumes of the two species increases, more negative excess molar volumes as well as excess isentropic compressibilities are observed [19].

3.3. Deviations in viscosity

The viscosity deviation, $\Delta\eta$, was calculated by using the relation,

$$\Delta\eta = \eta - \sum_i x_i \eta_i, \tag{4}$$

where η is the viscosity of the binary mixture and η_i are the viscosities of pure components. Table S3 in Supplementary material presents experimental values of viscosities and calculated values of viscosity deviations for the binary systems of triethyl phosphate with *N*-methylformamide, *N*,*N*-dimethylformamide and *N*,*N*-dimethylacetamide at 298.15 K.

Fig. 4 shows viscosity deviations as functions of mole fraction of TEP for the studied systems. It is evident that values of viscosity deviations for all mixtures are positive and small in magnitude over the entire composition range.

It is known that the viscosity deviation is related to the resistance of a mixture to flow [43]. Therefore, positive deviations in viscosity values observed for binary systems of triethyl phosphate with *N*,*N*-dimethylformamide and *N*,*N*-dimethylacetamide indicate that the resistance to flow of the mixture is higher than those of pure compounds. It seems to be the result of emergence of relatively weak dipole–dipole interactions between unlike molecules when mixture is created. More positive values of the viscosity deviations observed for TEP + DMF system in comparison to those for TEP + DMA mixtures confirm that stronger interactions exist between triethyl phosphate and *N*,*N*-dimethylformamide than between triethyl phosphate and *N*,*N*-dimethylacetamide molecules. As discussed above, the same effect was responsible for more negative excess molar volumes and excess isentropic compressibilities observed for the TEP + DMF system.

Further inspection of Fig. 4 reveals that the dependence of viscosity deviations for the TEP + NMF system differs from the others and is asymmetrical. For solutions with small content of triethyl phosphate viscosity deviations are significantly higher than those observed for *N*,*N*-dimethylformamide and *N*,*N*-dimethylacetamide. When molar fraction of triethyl phosphate reaches the value ~0.2, $\Delta\eta$ starts to decrease sharply and at molar fraction ~0.4 it becomes lower than that observed for DMA and DMF. This behavior can be explained by two opposite effects, i.e., of forming and destroying hydrogen bonds when component are mixed. When TEP is added to NMF the forming of new specific interactions between unlike molecules seems to dominate and the relatively high positive viscosity deviations are observed. However, when concentration of triethyl phosphate is high enough the destroying of hydrogen bonds between NMF molecules makes the flow easier and as the result

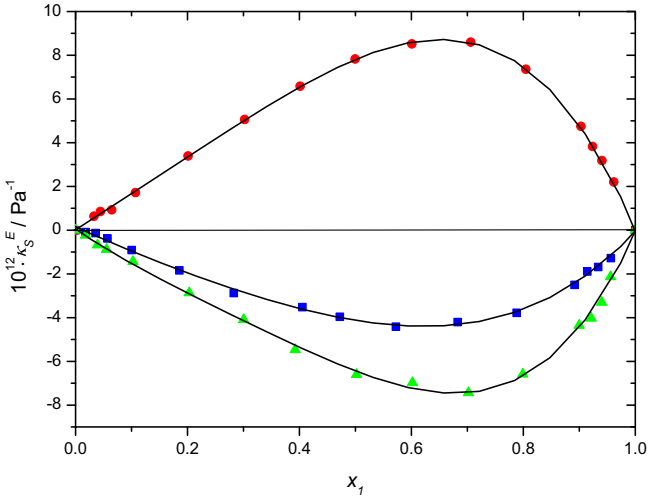

Fig. 3. Excess isentropic compressibility, κ_S^E, for triethyl phosphate (1) + amide (2) at p = .1 MPa as a function of mole fraction, x_1, at T = 298.15 K: ● (red), *N*-methylformamide; ■ (blue), *N*,*N*-dimethylacetamide; ▲ (green), *N*,*N*-dimethylformamide; —, Eq. (6).

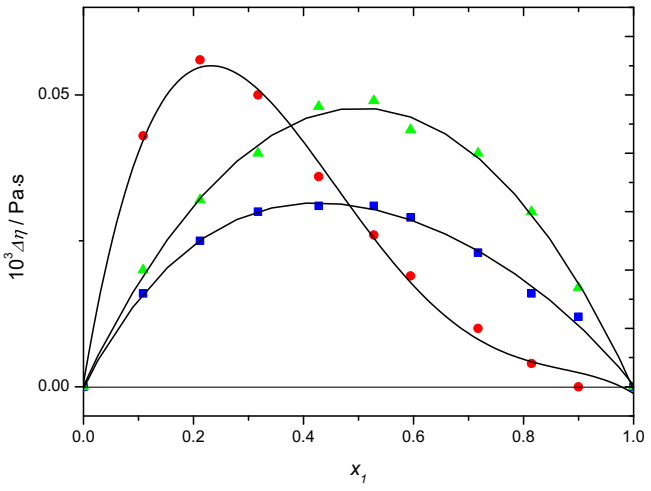

Fig. 4. Viscosity deviations, $\Delta\eta$, for triethyl phosphate (1) + amide (2) at p = 0.1 MPa as a function of mole fraction, x_1, at T = 298.15 K: ● (red), *N*-methylformamide; ■ (blue), *N*,*N*-dimethylacetamide; ▲ (green), *N*,*N*-dimethylformamide; —, Eq. (6).

viscosity deviations become to be smaller. Thus, one can say that, the for the TEP + NMF system the effect due to the breaking up of the self-associated structure of pure *N*-methylformamide is dominant over the effect of hydrogen bonding and dipole–dipole interactions between unlike molecules. This conclusion is in agreement with our findings from the density and sound velocity measurements.

Furthermore, as seen from Table S3, only for mixtures of triethyl phosphate and *N*-methylformamide the maximum of viscosity is observed. Similar effects were observed for mixtures of *N*,*N*-dimethylformamide and water [44]. Since the occurrence of maxima indicates stronger interactions between components of solutions, the viscosity dependence confirms that in TEP + NMF system specific interactions such as hydrogen bonds can be formed [43]. The lack of viscosity maximum for TEP + DMA and TEP + DMF indicates that only dipole–dipole interactions between unlike molecules can be formed.

The measured viscosities and densities of binary mixtures allowed us to calculate the excess Gibbs energy of activation for viscous flow, ΔG^E, using the equation,

$$\Delta G^E = RT[\ \ln(\eta V) - (x_1\ \ln(\eta_1 V_1) + x_2\ \ln(\eta_2 V_2))] \tag{5}$$

where R is the gas constant, T is the absolute temperature and V is the molar volume of the mixture defined as $V = (x_1M_1 + x_2M_2)/d$. Fig. 5 presents the variation of ΔG^E versus x_1 for the triethyl phosphate mixtures. For all studied systems positive values of excess Gibbs energy of activation were found. Moreover, the values obtained for TEP + NMF and TEP + DMF are similar in magnitude, while for TEP + DMA mixtures significantly lower values are observed. As positive values of excess Gibbs energies of activation indicate specific interactions, i.e., dipole–dipole interactions and hydrogen bonds between unlike molecules, one can say that in all systems such effects are prevalent. The smaller values of ΔG^E obtained for mixtures of triethyl phosphate and *N*,*N*-dimethylacetamide again support the weaker dipole–dipole interactions than those for mixtures of triethyl phosphate and *N*,*N*-dimethylformamide.

3.4. Correlations of excess properties

In order to correlate the calculated excess molar volumes, excess isentropic compressibilities and deviations in viscosity with the composition, the Redlich–Kister polynomial equation was applied [45],

$$Y^E = x_1x_2\sum_{i=0}^{2} A_i(x_1 - x_2)^i, \tag{6}$$

where the A_i values are adjustable parameters. The standard deviation of fit σ is defined as,

$$\sigma = \left[\frac{\sum_i \left(V^E_{calc} - V^E_{exp}\right)^2_i}{N-n}\right]^{1/2}, \tag{7}$$

where N is the number of experimental data points and n is the number of the fitted parameters.

In Figs. 1, 2 and 3 the continuous lines represent the correlated values according to the Redlich–Kister polynomial. As it can be seen, the calculated values agree very well with the experimental data. The A_i values were determined using the least squares method and they are listed in Tables 3, 4 and 5 along with their standard deviations. Almost for all systems excess molar volumes, excess isentropic compressibilities and deviations in viscosity with composition were correlated using free-parameter Redlich–Kister polynomial equation. Only for viscosity deviations for triethyl phosphate and *N*-methylformamide a better fit was obtained for four-parameter Redlich–Kister polynomial equation.

3.5. Molecular dynamics simulations

3.5.1. Solvent structure

The radial distribution functions (RDFs) for the studied systems are presented in Figs. 6, 7, and 8 for TEP–TEP, amide–amide, and TEP–amide pairs, respectively. In each case the RDFs are based on the center of mass (CoM) separation between the molecules. It is quite apparent that for DMA and DMF the structure of both solvents in the mixture does not differ considerably with the changing composition of the mixture. On the other hand, significant changes in the short-ranged structure are noticeable in the case of the TEP + NMF mixture.

The TEP–TEP RDF (Fig. 6) for pure TEP reveals that the first solvation shell of a given TEP molecule has a clear double maximum structure, which can be connected with the anisotropy of the TEP molecule itself. The two maxima (at ~0.65 nm and ~0.77 nm) are related to the intermolecular contacts at the P═O site and at the alkyl chains end of the TEP molecule, respectively. The locations of these maxima do not change considerably in the case of the TEP + DMA and TEP + DMF series (viz. Fig. 6a and b) and the only visible influence of the ongoing dilution of TEP is the slightly diminishing intensity of the entire first peak, as expected from a simple fractional concentration effect. Slight changes in the long range order of TEP are also visible as TEP becomes displaced by progressively more amide molecules with decreasing x_1. On the contrary, in the case of the TEP + NMF series (see Fig. 6c) there is clear evidence that TEP looses its short range structure as the TEP–TEP contacts at the P═O site are replaced by the apparently more preferable TEP–NMF contacts. The influence of the TEP dilution on the long range order also seems to be the most profound in this case and the increasing RDF intensity at ~1 nm indicates that TEP molecules are being gradually pulled away from each other, which is an indirect proof of the increasing homogeneity of the mixtures.

The observations based on the TEP–TEP RDFs are further corroborated by the amide–amide RDFs (Fig. 7). In particular, the latter reveal a virtually unchanged first solvation shell of the amide component with respect to the bulk amide in the case of DMA and DMF. The first peak in the RDF (at ~0.61 nm and ~0.55 nm for DMA and DMF, respectively) does not change significantly either its position or intensity. Interestingly, while the second solvation shell maintains its average intermolecular separation (at ~1.03 nm and ~0.97 nm for DMA and DMF, respectively), it becomes increasingly compressed with increasing

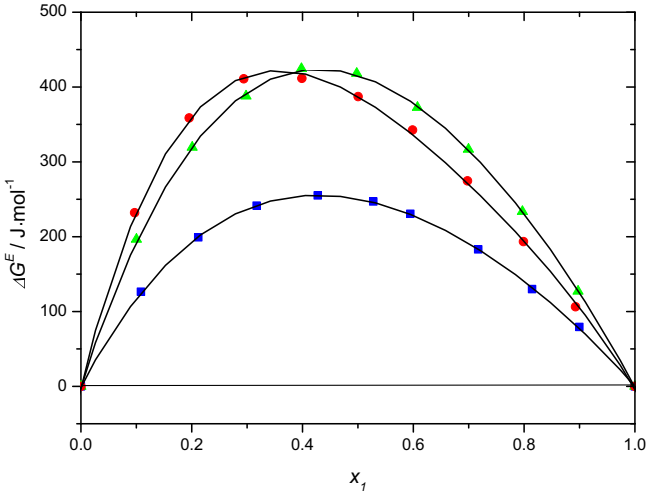

Fig. 5. Excess Gibbs energy of activation for viscous flow, ΔG^E, for triethyl phosphate (1) + amide (2) at $p = 0.1$ MPa as a function of mole fraction, x_1, at $T = 298.15$ K: ● (red), *N*-methylformamide; ■ (blue), *N*,*N*-dimethylacetamide; ▲ (green), *N*,*N*-dimethylformamide; —, Eq. (6).

Table 3
Adjusted parameters A_i and standard deviation of Eq. (6) for $10^6 \cdot V^E/(m^3 \cdot mol^{-1})$ at temperatures investigated.

T/K	A_o	A_1	A_2	σ
TEP + DMA				
293.15	−0.0436	0.0299	−0.0108	0.0002
298.15	−0.0519	0.0344	−0.0133	0.0003
303.15	−0.0613	0.0408	−0.0067	0.0003
308.15	−0.0672	0.0363	−0.0105	0.0004
TEP + DMF				
293.15	−0.217	0.095	−0.016	0.002
298.15	−0.217	0.094	−0.019	0.002
303.15	−0.218	0.090	−0.022	0.002
308.15	−0.217	0.088	−0.022	0.003
TEP + NMF				
293.15	1.488	−0.354	0.002	0.002
298.15	1.484	−0.351	0.0002	0.002
303.15	1.477	−0.353	−0.008	0.002
308.15	1.469	−0.351	−0.015	0.002

x_1 as indicated by the gradual disappearance of the tail at long r of the second peak in the respective RDFs. Simultaneously, a more pronounced amide–amide third solvation shell develops, further signifying the overall compression of the amide structure which is suggestive of the microheterogeneity of the TEP + DMA and TEP + DMF mixtures. Once again the TEP + NMF series clearly stands out, as the first solvation shell of NMF becomes very significantly perturbed with respect to the bulk amide with increasing x_1. The shoulder at low r in the first peak quickly disappears, while the first maximum shifts gradually from ~0.49 nm for $x_1 = 0$ to ~0.54 nm for $x_1 = 0.9$. We note here that the discussed shoulder is clearly attributable to the NMF–NMF pairs forming hydrogen bonds (see below for H-bonding analysis), as the average CoM separation for such pairs is ca. 0.44 nm, in accordance with the position of the observed shoulder. A similar maximum shift is also observed for the second peak in the RDF, indicating that the second neighbors are also being pulled apart from each other and further confirming the strongly homogeneous character of the TEP + NMF mixture.

The TEP–amide RDFs (Fig. 8) also reveal a much higher tendency for mutual interactions between TEP and the amide component for the TEP + NMF mixtures. For the TEP + DMA and TEP + DMF systems the first peak in the RDF only slightly changes with the mixture composition and the RDF series look overall very similar. In fact, by scaling the r variable by ~1.05 for the TEP + DMF series a very accurate overlap between the TEP + DMA and TEP + DMF RDFs can be obtained, irrespective of the mixture composition. This shows that the observed differences stem from the different molecular size of the amide component only. In strike contrast, the TEP + NMF RDFs display a very prominent first peak, signifying the importance of the first solvation shell contacts between TEP and NMF molecules. The height of the first peak initially increases considerably with x_1, but remains roughly constant for $x_1 \geq 0.4$, indicating a stabilization of the mode of interaction at this particular composition. An opposite behavior can be observed in the NMF–NMF RDFs (cf. Fig. 7c) that are in turn very similar for $x_1 \leq 0.3$, a further proof that amide–amide interactions become less preferable than interactions with TEP with increasing x_1. These observations are in remarkable agreement with the experimentally measured viscosity deviations (see Fig. 4) that become the least positive for the TEP + NMF system starting at $x_1 > 0.4$. This can be interpreted as the formation of stable NMF–TEP H-bonded complexes that destroy the neat NMF structure and do not hinder the viscous flow dramatically with respect to the bulk TEP.

In order to quantify the observed preferences for intermolecular interactions we apply the preferential solvation concept to our two-component systems [46]. In such system, the preference of the molecule 1 to interact with itself rather than the second component may be described by the preferential solvation index,

$$\delta_{11} = x_1^{local} - x_1, \tag{8}$$

where x_1^{local} is the *local* mole fraction of molecule 1 around reference molecule 1. In general, positive values of δ_{11} indicate a tendency for self-association, while negative values signify strong interactions between the components. In an ideal solution $\delta_{11} = 0$, which is also true in the long distance limit for real solutions [46,47].

The preferential solvation indices are most accurately derived from Kirkwood–Buff integrals [46–48]. The latter can be strictly obtained from the experimental thermodynamic data [48], but their application to molecular simulations is problematic due to their extremely slow

Table 4
Adjusted parameters A_i and standard deviation of Eq. (6) for $10^{10} \cdot \kappa_S^E/Pa^{-1}$ at 298.15 K.

Binary mixture	A_o	A_1	A_2	σ
TEP + DMA	−0.175	0.088	−0. 036	0.002
TEP + DMF	−0.260	0.193	−0. 096	0.003
TEP + NMF	0.217	−0.143	0.033	0.001

Table 5
Adjusted parameters A_i and standard deviation of Eq. (6) for $10^3 \cdot \Delta\eta/(Pa \cdot s)$ at 298.15 K.

Binary mixture	A_o	A_1	A_2	A_3	σ
TEP + DMA	0.123	−0.035	0.025	–	0.001
TEP + DMF	0.192	−0.014	0.006	–	0.001
TEP + NMF	−0.226	−0.864	0.222	−0.166	0.002

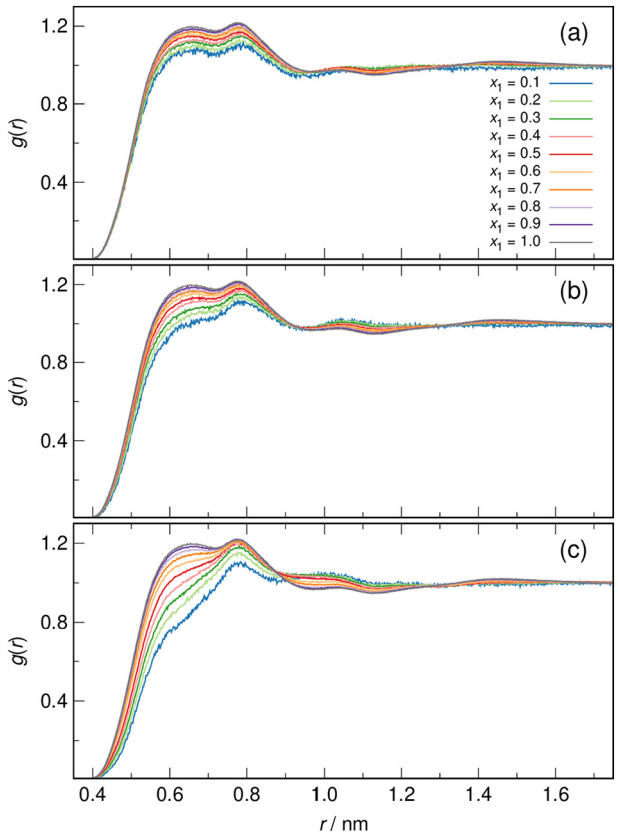

Fig. 6. The TEP–TEP radial distribution functions based on the center of mass separation for (a) TEP + DMA, (b) TEP + DMF and (c) TEP + NMF mixtures. See panel (a) for the color code for mixture compositions (x_1).

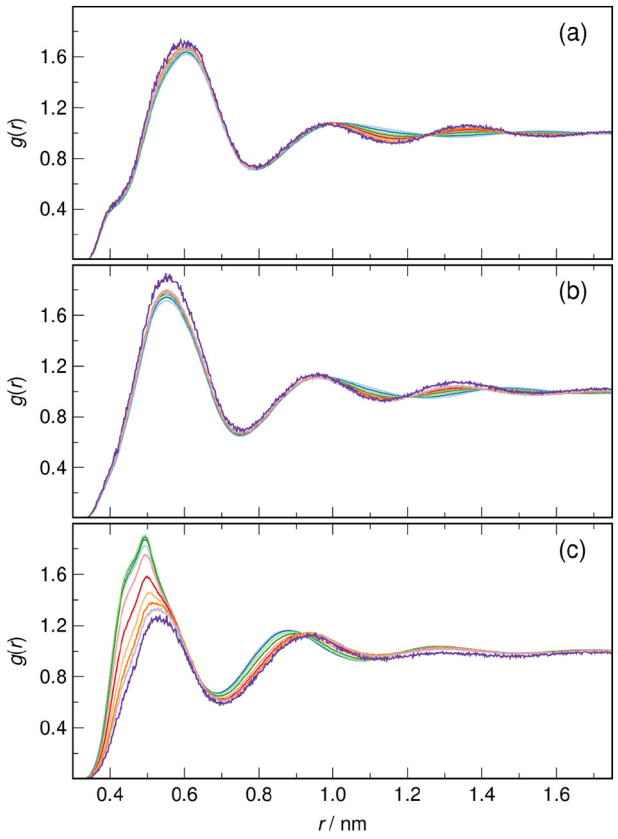

Fig. 7. The amide–amide radial distribution functions based on the center of mass separation for (a) TEP + DMA, (b) TEP + DMF and (c) TEP + NMF mixtures. See Fig. 6a for the color code for mixture compositions (x_1).

convergence with r and the fact that they are only defined for open systems (i.e., they require a grand canonical ensemble simulation) [46]. As a workaround, we use a definition based solely on the local coordination number [47]. Thus, we define the local amide–amide preferential solvation index, δ_{AA}, as,

$$\delta_{AA}(r) = \frac{N_{22}(r)}{N_{22}}(r) + N_{21}(r) - x_2, \tag{9}$$

where $N_{22}(r)$ is the number of amide molecules around a reference amide molecule up to the distance r, while $N_{21}(r)$ is the respective number of TEP molecules. Note that these coordination numbers are obtained by the integration of the respective $g(r)$ functions shown in Figs. 7 and 8.

The distance dependence of the δ_{AA} factors in the studied systems is shown in Fig. 9 for two selected compositions ($x_1 = 0.4$ and $x_1 = 0.8$). At low r values, δ_{AA} is uniformly positive even at large amide dilutions, simply because the smaller amide molecules are able to come in closer contact with each other than with the bulkier TEP molecule. However, the intermediate intermolecular separation regime (up to $r \approx 1$ nm) reveals important differences between DMA and DMF on the one hand and NMF on the other hand. For the dimethyl substituted amides δ_{AA} remains positive up to $r \approx 0.8$ nm even in the presence of large excess of TEP, meaning that these amides prefer self-association and the structure of the solutions is consequently micro-heterogeneous. This explains the very small negative excess molar volumes observed experimentally are most probably due to a simple packing effect. On the contrary, in the TEP–NMF system for $x_1 \geq 0.4$ δ_{AA} is negative from $r \approx 0.55$ nm up to and beyond 1 nm, signifying the crucial importance of the interactions between the components of the mixture. The large positive excess molar volumes are then presumably a result of the "stiffness" of the TEP–NMF complexes that form in the mixture and that fit poorly in the bulk structure of the components. It also provides an explanation to the large and positive excess compressibilites observed experimentally that result from the same rigidity of the TEP–NMF complexes that provides resistance to the compression of the system even though the void volume is large.

3.5.2. Hydrogen bonding in NMF solutions

In order to shed more light on the nature of intermolecular interactions between the components of the just discussed system, we focus now on the most obvious difference separating it from the doubly substituted amides, namely the presence of amide hydrogen in NMF that is able to form H-bonds in solution. We performed H-bond analysis in the TEP + NMF system applying the conventional definition of an H-bond based on the distance between heavy atoms (nitrogen and oxygen) and the angle formed between the N—H and N···O vectors [49]. In particular, we use $r_{NO} \leq 0.35$ nm and $\beta_{HNO} \leq 30°$ as the criteria for the H-bond existence. All results of the H-bond analysis are summarized in Fig. 10.

We first focus on the distribution of the H-bonds between the acceptor species (see Fig. 10a). In the TEP + NMF system a donor NMF molecule can form an H-bond to either NMF or TEP molecule as an acceptor. Alternatively, no H-bond can be formed by a particular NMF molecule, resulting in a dangling N—H group. In bulk liquid NMF we find that 77% N—H groups act on average as H-bond donors, which results in 1.54H-bonds per NMF molecule, in adequate agreement with the experimental data (1.8 ± 0.2 [35]). The fraction of non-H-bonded NMF diminishes with x_1 as it starts to preferentially form H-bonds to TEP. This preference is immediately detectable, as already at $x_1 = 0.3$ more H-bonds are formed to TEP than NMF as an acceptor. The fraction of non-H-bonded NMF molecules reaches a limiting value of ~0.05 at $x_1 = 0.8$, when also almost all NMF molecules become H-bonded to TEP.

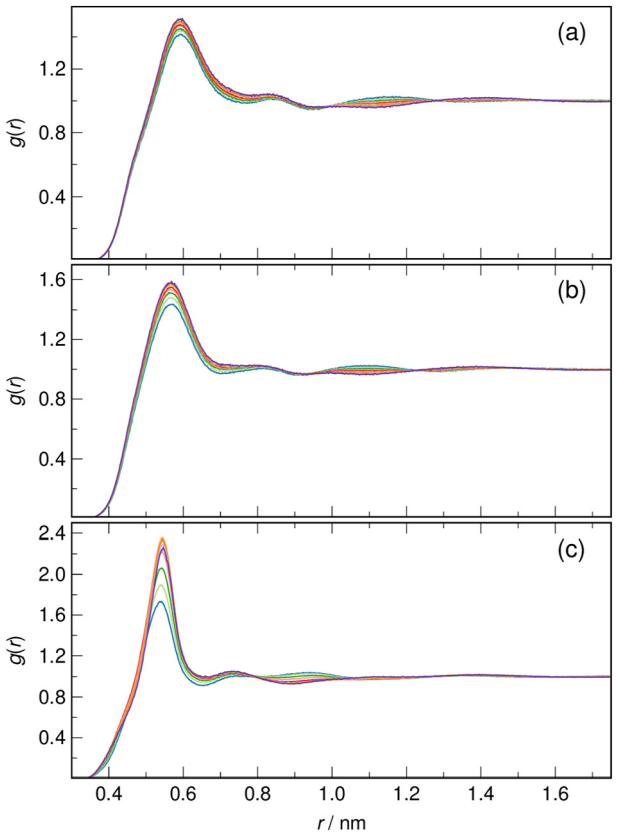

Fig. 8. The TEP–amide radial distribution functions based on the center of mass separation for (a) TEP + DMA, (b) TEP + DMF and (c) TEP + NMF mixtures. See Fig. 6a for the color code for mixture compositions (x_1).

In order to quantify the observed tendency of NMF to prefer TEP as an H-bond acceptor, we apply a concept similar to the preferential solvation index discussed above (Eq. (9)). Namely, we define the preferential hydrogen bond index, δ_{HB}, as,

$$\delta_{HB} = \frac{N_{HB}(\text{NMF–TEP})}{N_{HB}}(\text{NMF–TEP}) + N_{HB}(\text{NMF–NMF}) - x_1, \quad (10)$$

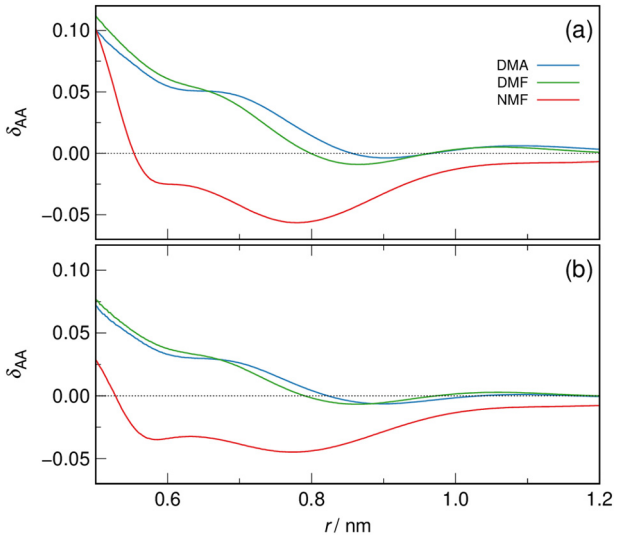

Fig. 9. The distance dependence of the amide–amide preferential solvation index, δ_{AA}, for TEP + DMA (blue), TEP + DMF (green) and TEP + NMF (red) mixtures at (a) $x_1 = 0.4$ and (b) $x_1 = 0.8$.

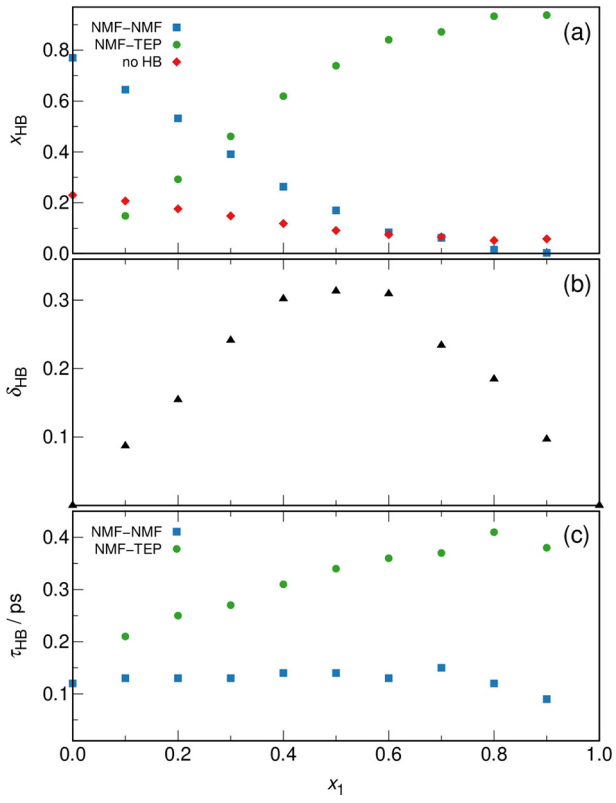

Fig. 10. Selected H-bonding characteristics in the TEP + NMF system: (a) the fraction of NMF molecules H-bonded to NMF, ■ (blue), H-bonded to TEP, ● (green), and not engaged in H-bonding, ◆ (red), (b) the preferential hydrogen bond index, and (c) the H-bond persistence time for NMF molecules H-bonded to NMF, ■ (blue), and H-bonded to TEP, ● (green).

where N_{HB} is the average number of H-bonds of the given type. If H-bonding in the mixture is purely random, than $\delta_{HB} = 0$, while positive (negative) values of it would indicate the preference for the formation of NMF–TEP (NMF–NMF) H-bonds.

As seen in Fig. 10b, the preferential H-bond index is uniformly positive across the entire composition range. Its considerable magnitude implies that the P═O group of TEP is a much better H-bond acceptor than the C═O group of NMF. Most importantly, the shape of the dependence of δ_{HB} on x_1 is roughly symmetrical around $x_1 = 0.5$ where it shows a maximum. Remarkably, the discussed dependence follows the course of the experimentally determined excess molar volumes. Thus, the main reason for the positive values of the latter in the TEP + NMF system is the formation of rigid H-bonded complexes between NMF and TEP that are statistically most preferable around the equimolar composition of the mixture.

Finally, we determined the mean H-bond persistence time from our H-bonding data based on the H-bond population operator, $h(t)$, that is a step function with a value of 1 if a tagged NMF molecule is an H-bond donor at time t and 0 otherwise. In turn, its continuous version, $H(t)$, has a value of 1 if a tagged NMF molecule acts as an H-bond donor *continuously* in the time period [0; t]. The latter indicator lets us define the desired mean H-bond persistence time as an integral of a time correlation function [50],

$$\tau_{HB} = \int_0^t \frac{\langle h(0)H(t)\rangle}{\langle h(0)\rangle} dt, \quad (11)$$

where ⟨⟩ denotes an ensemble average over all bonds present at $t = 0$.

As seen in Fig. 10c, the H-bond persistence time for NMF–NMF H-bonds is approximately constant up to $x_1 = 0.8$ ($\tau_{HB} \approx 0.13$ ps) and

falls only for the most diluted mixture. On the other hand, the NMF–TEP H-bonds are clearly more persistent. For them, τ_{HB} is already 1.5 times greater than for NMF–NMF H-bonds at $x_1 = 0.1$ and it raises linearly with x_1 up to $x_1 = 0.8$, when it seems to stabilize at ~0.4 ps (i.e., three times as much as for NMF–NMF H-bonds). It is evident then that the NMF–TEP H-bonds are not only more preferred in the discussed system, but are also characterized by significantly longer lifetimes.

There is an apparent discrepancy between the trend of the preferential H-bond index and the H-bond persistence time with x_1, as clearly seen in Fig. 10. However, the two properties signify related, but distinct phenomena. While the preferential H-bond index describes deviations from random preference for H-bond acceptor in the TEP + NMF system and is thus a static descriptor, the H-bond persistence time is a dynamic property related to the kinetics of the H-bond breaking process. Therefore, they do not necessarily capture the same phenomena in the studied system. The persistence time is additionally clearly coupled to the H-bond energetics as inferred from vibrational spectra; see below.

Vibrational spectroscopy is a potent technique for studying H-bonding in liquid NMF and its complexes [51]. In order to study the effect of the differing H-bonding environments in the TEP + NMF system, we apply vibrational density of states (VDOS) also known as power spectrum that allows investigation of vibrational frequencies independently of infrared and Raman selection rules [52]. VDOS is usually defined as the Fourier transform of the time correlation function of the mass-weighted particle velocities [52], i.e.,

$$I(\omega) = \int_{-\infty}^{\infty} \langle u_k(0) u_k(t) \rangle e^{-i\omega t} dt, \tag{12}$$

where $u_k(t)$, is the mass-weighted velocity of atom k at time t, $u_k(t) = m_k^{1/2} v_k(t)$, and $\langle\rangle$ denotes an ensemble average over all atoms.

In Fig. 11 the power spectra in the ν_{NH} stretching vibration range that is sensitive to local H-bonding are shown for the studied TEP + NMF mixtures. In bulk liquid NMF, the maximum position of the discussed band is 3321 cm^{-1}, in good agreement with the experimental data (3300 cm^{-1} [53,54]). As the fraction of NMF in the mixture becomes lower, the intensity of the band naturally falls due to the progressively smaller number of N—H oscillators. At the same time, however, the band shifts noticeably red and its maximum position reaches a limiting value of 3308 cm^{-1} in diluted solutions of NMF. The red shift of the proton stretching vibration is a sensitive indicator of the increasing strength in N–H···O H-bonds [55].

Additionally, the maximum position of the ν_{NH} stretching vibration band clearly correlates with the NMF–TEP H-bond persistence time determined above (see Fig. 10c), as seen in the inset in Fig. 11, thus signifying the dynamic nature of the latter and its distinct relation to the H-bond strength. Ultimately, we can confirm that the stabilizing effect of the NMF–TEP H-bonding is the key factor determining the thermodynamic properties in this system and making it unique in comparison to dimethyl amide derivatives.

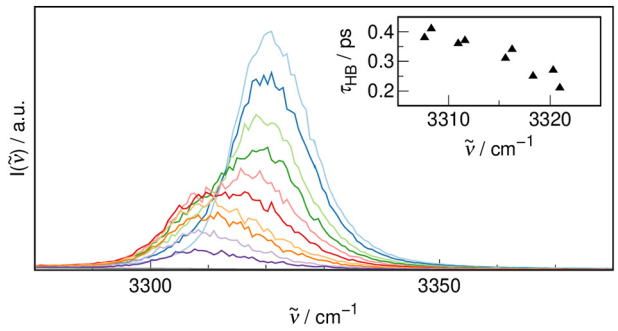

Fig. 11. The vibrational density of states for TEP + NMF mixtures in the ν_{NH} stretching vibration range. See Fig. 6a for the color code for mixture compositions (x_1). (Inset) The dependence of the H-bond persistence time for NMF molecules H-bonded to TEP (see Fig. 10) on the position at maximum of the ν_{NH} stretching band of NMF.

4. Conclusions

From the experimental data of density at the temperatures (293.15, 298.15, 303.15 and 308.15) K and viscosity and ultrasonic velocity at 298.15 K, the values of excess molar volume, excess isentropic compressibility, viscosity deviation and excess Gibbs energy of activation for viscous flow for mixtures of triethyl phosphate and *N*-methylformamide, *N*,*N*-dimethylacetamide and *N*,*N*-dimethylformamide have been calculated. The Redlich–Kister-type polynomial equation was used to correlate the results. The viscosity deviations and the excess Gibbs energy were found to be positive for the all systems investigated, while the excess volumes and the excess isentropic compressibilities were negative for TEP + DMA and for TEP + DMF systems, and positive for TEP + NMF systems. The results indicate that triethyl phosphate acts as structure breaker for self-associated *N*-methylformamide. In mixtures with *N*,*N*-dimethylacetamide and *N*,*N*-dimethylformamide, i.e., solvents which cannot act as hydrogen bond donors, dipole–dipole interactions are responsible for negative values of the excess volumes and the excess isentropic compressibilities. Moreover, the thermodynamic properties obtained from density, sound velocity and viscosity measurements indicate the stronger interactions between triethyl phosphate and *N*,*N*-dimethylformamide than those between triethyl phosphate and *N*,*N*-dimethylacetamide molecules.

Molecular dynamics simulations were crucial for providing the explanation for the composition dependence of the experimentally determined excess properties, particularly the striking differences observed between the dimethyl substituted amides on the one hand and NMF on the other hand. It was revealed that in the TEP + DMA and TEP + DMF systems the unlike molecular interactions are less preferable than self-interactions, as indicated by the strongly positive preferential solvation index values. Consequently, the structure of these mixtures is micro-heterogeneous and the observed very small negative excess molar volumes and negative excess molar compressibilities are attributable to a packing effect. On the other hand, the TEP + NMF system stands out due to the ability of *N*-methylformamide to donate H-bonds preferentially to the TEP molecules. The resulting H-bonded complexes are rigid and longer-lived than in pure NMF and poorly accommodate into the bulk structure of both solvents, thus leading to positive excess molar volume and excess isentropic compressibility in this system.

CRediT authorship contribution statement

Dorota Warmińska: Methodology, Investigation, Formal analysis, Writing - original draft. **Maciej Śmiechowski:** Resources, Investigation, Formal analysis, Writing - original draft.

Declaration of competing interest

The authors declare that they have no known competing financial interests or personal relationships that could have appeared to influence the work reported in this paper.

Acknowledgements

Calculations were performed at the Academic Computer Center in Gdańsk (TASK). This research was supported by the statutory fund of the Chemical Faculty, Gdańsk University of Technology.

Appendix A. Supplementary data

Supplementary data to this article can be found online at https://doi.org/10.1016/j.molliq.2020.112778.

References

[1] K. Xu, M.S. Ding, S. Zhang, J.L. Allen, T.R. Jow, An attempt to formulate nonflammable lithium ion electrolytes with alkyl phosphates and phosphazenes, J. Electrochem. Soc. 149 (2002) A622–A626.

[2] J. Chang, J. Zuo, L. Zhang, G.S. O'Brien, T.S. Chung, Using green solvent, triethyl phosphate (TEP), to fabricate highly porous PVDF hollow fiber membranes for membrane distillation, J. Membr. Sci. 539 (2017) 295–304.

[3] Q. Li, Z.L. Xu, L.Y. Yu, Effects of mixed solvents and PVDF types on performances of PVDF microporous membranes, J. Appl. Polym. Sci. 115 (2010) 2277–2287.

[4] K. Matsumoto, K. Inoue, K. Utsugi, A highly safe battery with a non-flammable triethyl-phosphate-based electrolyte, J. Power Sources 273 (2015) 954–958.

[5] B.S. Lalia, N. Yoshimoto, M. Egashira, M. Morita, A mixture of triethylphosphate and ethylene carbonate as a safe additive for ionic liquid-based electrolytes of lithium ion batteries, J. Power Sources 195 (2010) 7426–7431.

[6] J.J. Comor, M.M. Kopecni, Excess and partial excess molar volumes of mixing trimethyl- and triethylphospate with water, J. Solut. Chem. 20 (1991) 945–953.

[7] J.C. Bollinger, G. Yvernault, T. Yvernault, Physical properties of the solvent mixtures triethylphosphate + hexamethylphosphoric triamide at 25°C, J. Solut. Chem. 7 (1978) 317–324.

[8] J. Wawer, A. Płaczek, D. Warmińska, W. Grzybkowski, Usefulness of the Free Length Theory for assessment of the self-association of pure solvents, J. Mol. Liq. 149 (2009) 37–44.

[9] S. Kannan, K. Kishore, Absolute viscosity and density of trisubstituted phosphoric esters, J. Chem. Eng. Data 44 (1999) 649–655.

[10] C. Caleman, P.J. van Maaren, M. Hong, J.S. Hub, L.T. Costa, D. van der Spoel, Force field benchmark of organic liquids: density, enthalpy of vaporization, heat capacities, surface tension, isothermal compressibility, volumetric expansion coefficient, and dielectric constant, J. Chem. Theory Comput. 8 (2012) 61–74.

[11] S. Mrad, C. Lafuente, M. Hichri, I. Khattech, Density, speed of sound, refractive index, and viscosity of the binary mixtures of *N,N*-dimethylacetamide with methanol and ethanol, J. Chem. Eng. Data 61 (2016) 2946–2953.

[12] D. Warmińska, D. Lundberg, Solvation of alkaline earth metal ions in *N,N*-dimethylformamide and *N,N*-dimethylacetamide – a volumetric and acoustic study, J. Chem. Thermodyn. 92 (2016) 108–117.

[13] T.M. Aminabhavi, B. Gopalakrishna, Density, viscosity, refractive index, and speed of sound in aqueous mixtures of *N,N*-dimethylformamide, dimethyl Sulfoxide, *N,N*-dimethylacetamide, acetonitrile, ethylene glycol, diethylene glycol, 1,4-dioxane, tetrahydrofuran, 2-methoxyethanol, and 2-ethoxyethanol at 298.15 K, J. Chem. Eng. Data 40 (1995) 856–861.

[14] M.N. Roy, I. Banik, D. Ekka, Physics and chemistry of an ionic liquid in some industrially important solvent media probed by physicochemical techniques, J. Chem. Thermodyn. 57 (2013) 230–237.

[15] J.A. Riddick, W.B. Bunger, T.K. Sakano, Organic solvents: physical properties and methods of purification, Wiley, New York, 1986.

[16] P. Venkatesu, M.J. Lee, H.M. Lin, Volumetric properties of (*N,N*-dimethylformamide + aliphatic diethers) at temperatures ranging from (298.15 to 358.15) K, J. Chem. Thermodyn. 37 (2005) 996–1002.

[17] A. Płaczek, H. Koziel, W. Grzybkowski, Apparent molar compressibilities and volumes of some 1,1-electrolytes in *N,N*-dimethylacetamide and *N,N*-dimethylformamide, J. Chem. Eng. Data 52 (2007) 699–706.

[18] S. Taniewska-Osinska, A. Piekarska, A. Kacperska, Viscosities of NaI in water-formamide and water-*N,N*-dimethylformamide mixtures from 5 to 45°C, J. Solut. Chem. 12 (1983) 717–727.

[19] P.K. Pandey, A. Awasthi, A. Awasthi, Acoustic, volumetric and spectroscopic investigations in binary mixtures of formamide + N-methylformamide + 2-chloroethanol at various temperatures, J. Mol. Liq. 187 (2013) 343–349.

[20] K.J. Han, J.H. Oh, S.J. Park, J. Gmehling, Excess molar volumes and viscosity deviations for the ternary system *N,N*-dimethylformamide + N-methylformamide + water and the binary subsystems at 298.15 K, J. Chem. Eng. Data 50 (2005) 1951–1955.

[21] D. Papamatthaiakis, F. Aroni, V. Havredaki, Isentropic compressibilities of (amide + water) mixtures: a comparative study, J. Chem. Thermodyn. 40 (2008) 107–118.

[22] P.S. Sikdar, Physico-chemical exploration of solution behaviour of some metal perchlorates prevailing in N-methyl formamide with the manifestation of ion solvent consequences, Thermochim. Acta 607 (2015) 53–59.

[23] M.J. Abraham, T. Murtola, R. Schulz, S. Páll, J.C. Smith, B. Hess, E. Lindahl, GROMACS: high performance molecular simulations through multi-level parallelism from laptops to supercomputers, SoftwareX 1 (2015) 19–25.

[24] W.L. Jorgensen, D.S. Maxwell, J. Tirado-Rives, Development and testing of the OPLS all-atom force field on conformational energetics and properties of organic liquids, J. Am. Chem. Soc. 118 (1996) 11225–11236.

[25] W.L. Jorgensen, J. Tirado-Rives, Potential energy functions for atomic-level simulations of water and organic and biomolecular systems, Proc. Natl. Acad. Sci. U. S. A. 102 (2005) 6665–6670.

[26] D. van der Spoel, P.J. van Maaren, C. Caleman, GROMACS molecule & liquid database, Bioinformatics 28 (2012) 752–753.

[27] U. Essmann, L. Perera, M.L. Berkowitz, T. Darden, H. Lee, L.G. Pedersen, A smooth particle mesh Ewald method, J. Chem. Phys. 103 (1995) 8577–8593.

[28] S. Páll, B. Hess, A flexible algorithm for calculating pair interactions on SIMD architectures, Comput. Phys. Commun. 184 (2013) 2641–2650.

[29] W.C. Swope, H.C. Andersen, P.H. Berens, K.R. Wilson, A computer simulation method for the calculation of equilibrium constants for the formation of physical clusters of molecules: application to small water clusters, J. Chem. Phys. 76 (1982) 637–649.

[30] S. Nosé, A unified formulation of the constant temperature molecular dynamics methods, J. Chem. Phys. 81 (1984) 511–519.

[31] W.G. Hoover, Canonical dynamics: equilibrium phase-space distributions, Phys. Rev. A 31 (1985) 1695–1697.

[32] G.J. Martyna, M.E. Tuckerman, D.J. Tobias, M.L. Klein, Explicit reversible integrators for extended systems dynamics, Mol. Phys. 87 (1996) 1117–1157.

[33] G.J. Martyna, D.J. Tobias, M.L. Klein, Constant pressure molecular dynamics algorithms, J. Chem. Phys. 101 (1994) 4177–4189.

[34] M. Basu, T. Samanta, D. Das, Volumetric and compressibility studies on tri-n-butyl phosphate (TBP)-phase modifier (1-octanol, 1-decanol and isodecanol) interactions from $T =$ (298.15 to 323.15) K, J. Chem. Thermodyn. 70 (2014) 1–12.

[35] F. Hammami, S. Nasr, M. Oumezzine, R. Cortès, H-bonding in liquid N-methylformamide as studied by X-ray scattering, Biomol. Eng. 19 (2002) 201–205.

[36] W.L. Jorgensen, C.J. Swenson, Optimized intermolecular potential functions for amides and peptides. Structure and properties of liquid amides, J. Am. Chem. Soc. 107 (1985) 569–578.

[37] T. Yonezawa, I. Morishima, Self-association of *N,N*-dimethylformamide, *N,N*-dimethylacetamide, and N-methylpyrrolidone, Bull. Chem. Soc. Jpn. 39 (1966) 2346–2352.

[38] F.S. Mortimer, Vibrational assignment and rotational isomerism in some simple organic phosphates, Spectrochim. Acta 9 (1957) 270–281.

[39] M. Roses, C. Rafols, J. Ortega, E. Bosch, Solute-solvent and solvent-solvent interactions in binary solvent mixtures. Part 1. A comparison of several preferential solvation models for describing ET(30) polarity of bipolar hydrogen bond acceptor-cosolvent mixtures, J. Chem. Soc. Perkin Trans. 2 (1995) 1607–1615.

[40] L. George, K. Sankaran, K.S. Viswanathan, C.K. Mathews, Matrix-isolation infrared spectroscopy of organic phosphates, Appl. Spectrosc. 48 (1994) 7–12.

[41] G.C. Benson, O. Kiyohara, Evaluation of excess isentropic compressibilities and isochoric heat capacities, J. Chem. Thermodyn. 11 (1979) 1061–1064.

[42] Y. Marcus, The Properties of Solvents, J. Wiley & Sons, Chichester, 1998.

[43] F. Nabi, M.A. Malik, C.G. Jesudason, S.A. Al-Thabaiti, A review of molecular interactions in organic binary mixtures, Korean J. Chem. Eng. 31 (2014) 1505–1517.

[44] E. Cherif, R. Jammazi, T. Othman, Thermodynamic properties of *N,N*-dimethylformamide + water, Phys. Chem. Liq. 52 (2014) 751–762.

[45] O. Redlich, A.T. Kister, Algebraic representation of thermodynamic properties and the classification of solutions, Ind. Eng. Chem. 40 (1948) 345–348.

[46] A. Ben-Naim, Preferential solvation in two- and in three-component systems, Pure Appl. Chem. 62 (1990) 25–34.

[47] H. Kokubo, B.M. Pettitt, Preferential solvation in urea solutions at different concentrations: properties from simulation studies, J. Phys. Chem. B 111 (2007) 5233–5242.

[48] J. Zielkiewicz, Preferential solvation of amides by methanol – a comparison of molecular dynamics calculations with the experimental data, TASK Q 5 (2001) 317–329.

[49] A. Luzar, D. Chandler, Hydrogen-bond kinetics in liquid water, Nature 379 (1996) 55–57.

[50] A. Luzar, Resolving the hydrogen bond dynamics conundrum, J. Chem. Phys. 113 (2000) 10663–10675.

[51] B. Jović, A. Nikolić, E. Davidović, S. Petrović, N–H···O hydrogen bonding. An FT-IR, NIR study of N-methylformamide–ether systems, J. Serb. Chem. Soc. 75 (2010) 157–163.

[52] M. Thomas, M. Brehm, R. Fligg, P. Vöhringer, B. Kirchner, Computing vibrational spectra from ab initio molecular dynamics, Phys. Chem. Chem. Phys. 15 (2013) 6608–6622.

[53] E. DeGraaf, G.B.B.M. Sutherland, Vibrational spectrum of N-methyl formamide, J. Chem. Phys. 26 (1957) 716–717.

[54] I. Suzuki, Infrared spectra and normal vibrations of N-methylformamides $HCONHCH_3$, $HCONDCH_3$, $DCONHCH_3$ and $DCONDCH_3$, Bull. Chem. Soc. Jpn. 35 (1962) 540–551.

[55] Z. Dega-Szafran, A. Hrynio, M. Szafran, A quantitative comparison of spectroscopic and energy data, in solution, of NHO and OHO hydrogen bonds and gas-phase proton affinities: complexes of pyridines and pyridine N-oxides with acetic acids, J. Mol. Struct. 240 (1990) 159–174.